Reac Kinet Mech Cat
DOI 10.1007/s11144-015-0935-z

Experimental, detailed, and global kinetic reaction model for NO oxidation over platinum/alumina catalysts

Travis Wentworth[2] · Sudarshan Loya[1] · Christopher Depcik[1] · Susan Stagg-Williams[2]

Received: 7 July 2015 / Accepted: 30 September 2015

Abstract The oxidation of nitric oxide (NO) is a critical step when promoting lean NO_x trap and selective catalytic reduction conversion effectiveness; hence, it is important to understand the fundamental reaction mechanism. This awareness of the detailed reaction mechanism allows for the determination of an appropriate global reaction rate expression for numerical simulation efforts in the automotive field. This work succinctly reviews the literature in this area and derives a global expression for NO oxidation from stoichiometry using the detailed reactions steps. In this version, the parameters used to simulate the global expression are derived from the kinetic theory of gases and the detailed study of each NO reaction step; ensuring the correct functional dependency of each reaction parameter. Moreover, the global model is adapted to simulate different surface morphologies. The effect of temperature and surface changes (dispersion, particle size) are included while determining the parameters, so that the same variables can be used over wide range of catalysts effectively. This work summarizes the literature of experimentally observed NO oxidation in terms of surface coverage, species concentration dependency, and temperature variation. Finally, the authors verify the global model by simulating experimental data obtained for catalysts with varying noble metal particle size. As a result, the adaptive global model predicts NO oxidation conversion with changes in surface morphologies at greater than 93 % accuracy for the experimental data taken.

Keywords Kinetics · Global · Detailed · Nitrogen oxides

✉ Christopher Depcik
depcik@ku.edu

[1] Department of Mechanical Engineering, University of Kansas, 3138 Learned Hall, 1530 W. 15th Street, Lawrence, KS 66045, USA

[2] Department of Chemical and Petroleum Engineering, University of Kansas, 4163 Learned Hall, 1530 W. 15th Street, Lawrence, KS 66045, USA

Published online: 06 October 2015

Introduction

In today's society, there is a significant need to decrease fuel consumption while reducing dependency on fossil fuels. This has led to an increase in demand for compression ignition (CI) and gasoline direct injected (GDI) engines because of their increased fuel economy relative to stoichiometric engines. However, current and future regulations on nitrogen oxides (NO_x) emissions are particularly challenging to meet, for these lean-burning engines [1–4]. Under the traditional stoichiometric operating conditions of a port fuel injected gasoline engine, carbon monoxide (CO), hydrogen (H_2), and hydrocarbon (HC) emissions exist in sufficient quantities to reduce NO_x emissions from the engine over a traditional three way catalyst (TWC). However, the lean exhaust of CI and GDI engines contains mainly oxygen (O_2) and nitrogen monoxide (NO) without any other reducing species in adequate quantities to react over the TWC. Since NO_x decomposition is difficult to facilitate in oxygen rich environments, a low cost solution for conversion of NO_x to N_2 and O_2 is required.

In order to overcome this issue, various indirect catalytic approaches have been studied for NO_x reduction. The most common methods are selective catalytic reduction (SCR) and lean NO_x traps (LNTs). While SCR devices have largely become the automotive industry standard, the prospect of LNTs operating without a secondary fueling infrastructure (i.e., Diesel Exhaust Fluid) make them an attractive option. LNTs operate in two phases; a lean phase is used for storing NO_x, whereas a rich phase provides regeneration of the catalyst and reduction of stored NO_x. Since LNTs prefer the storage of nitrogen dioxide (NO_2) as compared to NO, the oxidation of NO is a critical step during LNT operation [5–7]. Often an oxidation catalyst (OC) is placed upstream of LNT and SCR devices in order to facilitate NO_2 production from NO. This is because SCR devices also prefer to convert NO_2 (using ammonia) because of its greater oxidative capabilities. Of note, LNTs and OCs are often formulated using Pt/γ-alumina catalysts as the base with other metals added (e.g., barium for LNTs) to promote the desired reactions.

Even though LNTs and OCs are commercially produced, one can still improve their operation by reducing the amount of precious metals while increasing their NO_x conversion. In this area, various researchers have investigated NO oxidation over Pt/γ-alumina catalysts while describing detailed and global reaction mechanisms [7–20]. However, while reviews of the NO oxidation mechanism have been accomplished [12, 21], further depth and understanding is needed. Hence, this work summarizes the literature findings for the detailed reaction mechanism. Moreover, only a few papers discuss the global reaction mechanism for NO oxidation [7, 13, 14, 22–25]. This kinetic modeling option is a definite need in the automotive industry for computationally fast catalyst simulation tools [26]. While some efforts use a power law expression, only Bhatia et al. provided a global mechanism for NO oxidation and modeled the system using the same reaction rate expression [25]. The following global reaction rate derivation differs from the Bhatia version as it takes NO oxidation as written in Eq. 1 as this half order oxygen reaction rate dependence has been shown by a number of groups [27–30]. A simplified overall reaction rate

expression based upon this global reaction by Sampara et al. achieved acceptable results modeling NO oxidation for diesel oxidation catalysts (DOC) [30]:

$$NO + 0.5O_2 \underset{k_{-1}}{\overset{k_1}{\rightleftarrows}} NO_2 \quad (1)$$

There is no consensus in the literature with respect to the various parameters to be used in the reaction mechanism, such as surface coverage of O_2 and NO_2, or how the various parameters might change with temperature and catalyst surface properties (e.g., dispersion or particle size). As a result, this work aims to fill in the gaps in the literature by providing experimental conversion data for catalysts with different dispersion and particle sizes at the same reaction conditions (i.e., space, time, oxygen, and NO concentrations) along with a global reaction rate expression and corresponding parameter values. Finally, a novel approach to simulate aging within the global kinetic frame work is established wherein noble metal particle size and reaction temperatures are used to described changes in the catalyst surface and atomic surface coverages resulting from the aforementioned thermal aging and operating temperature variation.

This adaptive approach for determining parameters expands the use of a global reaction rate expression for different catalyst morphologies, and aging conditions [31, 32]. Furthermore, these values were derived from catalyst fundamentals, resulting in parameter changes that can be interpreted based upon the observed physical changes. It should be noted that both experimental and simulation efforts were performed in the absence of additional species like water and carbon dioxide in order to focus on the main goal of an NO oxidation study. Furthermore, only platinum is included as the reactive metal catalyst; whereas, for LNT devices other materials (e.g., barium) can significantly influence Pt particle size and dispersion, subsequently affecting NO oxidation. Hence, the model formulation presented is more suited towards an OC device, but can be used to gain insight into LNT operation. First, in order to understand NO oxidation in more detail, a succinct historical account is provided.

Historical review

Work on NO oxidation began in the 1980s and it has undergone substantial research since then [33, 34]. The reaction was found to be equilibrium limited with NO_2 production peaking around 623–643 K [10, 12]. This presence of NO_2 inhibits the reaction [23] and it was found that the rate is structure sensitive; it rises with an increase in platinum particle size (i.e., a decrease in Pt dispersion) [10, 12, 35, 36]. In addition, the NO oxidation rate will increase with platinum loading up to 2–4 % [37]. Finally, there is no definitive consensus in the literature on whether the reaction follows a Langmuir–Hinshelwood (L–H) or Eley–Rideal (E–R) reaction mechanism [7, 8, 11–15, 22, 23, 25].

With respect to the individual steps of the detailed mechanism, NO adsorbs molecularly on the platinum particle with nitrogen attaching to the platinum and its dissociation is substantially reduced in presence of oxygen [38–40]. Both oxygen

and nitrogen dioxide adsorb dissociatively on platinum within the range of reaction temperatures studied [41, 42]. Nitrogen dioxide is a strong sintering agent as compared to NO, which in turn is stronger than oxygen [43]. Oxygen tends to desorb above 650 K and desorption temperature decreases with increased platinum particle size. On the other hand, surface coverage of oxygen increases with temperature from 300 to 650 K [41]. Nearly all researchers agree on the following steps of NO oxidation given below.

$$\mathrm{NO} + \mathrm{Pt} \underset{k_{-2}}{\overset{k_2}{\rightleftarrows}} \mathrm{Pt} \cdot \mathrm{NO} \tag{2}$$

$$\frac{1}{2}\mathrm{O_2} + \mathrm{Pt} \underset{k_{-3}}{\overset{k_3}{\rightleftarrows}} \mathrm{Pt} \cdot \mathrm{O} \tag{3}$$

$$\mathrm{Pt} \cdot \mathrm{NO} + \mathrm{Pt} \cdot \mathrm{O} \underset{k_{-4}}{\overset{k_4}{\rightleftarrows}} \mathrm{Pt} \cdot \mathrm{NO_2} + \mathrm{Pt} \tag{4}$$

$$\mathrm{Pt} \cdot \mathrm{NO_2} \underset{k_{-5}}{\overset{k_5}{\rightleftarrows}} \mathrm{NO_2} + \mathrm{Pt} \tag{5}$$

Although there is debate in literature with respect to the L–H or the E–R reaction mechanism, in this effort, the authors observe that L–H is the preferred method for NO oxidation over the E–R mechanism [7, 44]. This is because NO_2 requires two sites to dissociate; hence, the forward reaction of NO oxidation should follow as the reverse of NO_2 dissociation [7, 10, 39]. In addition, the literature suggests that surface coverage of both NO and oxygen contributes to variations observed in the NO oxidation rate, further suggesting the L–H pathway [10, 14, 25, 28]. Finally, most researchers working in the field of NO oxidation and storage support the same pathway for generation of the global reaction rate expression [12, 14–16, 18, 19, 22, 25, 28].

Based upon the presented detailed reaction mechanism, the global reaction mechanism is developed in a latter part of this paper. In order to calibrate the kinetic parameters of this global mechanism, a Pt/γ-alumina catalyst was prepared and packed bed experiments were conducted.

Nomenclature

Variable	Description	Units
A	Adsorption pre-exponential	(atm^{-1})
A_{Pt}	Area of platinum site	$(\mathrm{m}^2\ \mathrm{site}^{-1})$
A	Constant of calibration	(−)
B	Constant of calibration	(−)
$\bar{C}$	Molar species concentration	$(\mathrm{mol\ m}^{-3})$
D	Particle size	(m)
D	Gas diffusivity	$(\mathrm{m}^2\ \mathrm{s}^{-1})$
E	Activation energy	$(\mathrm{J\ mol}^{-1})$

Variable	Description	Units
G_a	Geometric surface area per unit volume	(m^2 m^{-3})
G_{ca}	Catalytic surface area per unit volume	(m^2 m^{-3})
$\bar{h}$	Molar specific enthalpy	(J mol^{-1})
ΔH	Heat of adsorption	(J mol^{-1})
K	Reaction kinetics pre-exponential	(mol m^{-2} s^{-1})
K	Adsorption equilibrium	(atm^{-1})
m_a	Mass of molecule	(kg)
N_A	Avogadro's number ($6.02214179 \times 10^{23}$)	(mol^{-1})
v	Frequency of collision	(s^{-1})
$Pt \cdot O$	Adsorbed atomic oxygen on platinum	(−)
$Pt \cdot NO$	Adsorbed NO on platinum	(−)
$Pt \cdot NO_2$	Adsorbed NO_2 on platinum	(−)
P	Pressure	(atm)
R	Forward or reverse reaction rate	(varies)
$\bar{R}$	Molar gaseous reaction rate	(mol m^{-2} s^{-1})
R_u	Universal gas constant	(J mol^{-1} K^{-1})
S	Sticking coefficient	(−)
S^0	Initial sticking coefficient	(−)

Experimental

Catalyst samples

High surface area γ-alumina (Strem Chemicals) was conditioned by sintering at 1073 K for 24 h and sieved to a particle size <100 μm. The conditioned γ-alumina was impregnated with an aqueous solution of the Pt precursor (platinum diammine nitrite 5 wt% in aqueous ammonia, Strem Chemicals). Catalysts were produced using the incipient wetness impregnation technique. The Pt precursor was diluted to a solution volume equivalent to the total pore volume of the support. $Pt/\gamma\text{-}Al_2O_3$ was produced to contain a 1/100 ratio by weight. The catalyst was dried at 393 K for 24 h and sintered at temperatures between 873 and 1073 K in order to obtain varying catalyst dispersion and particle size.

Catalyst sintering was carried out in a Thermolyne 46,100 muffle furnace controlled by a Eurotherm 2408 temperature controller. During each of the sintering steps the ramp rate for heating was 1 K min^{-1} and the cooling rate was 5 K min^{-1}. Catalysts were held at the specified sintering temperature for 8 h. Sintering was conducted in a stagnant air environment.

Flow reactor set up

NO oxidation experiments were carried out in a quartz tube reactor of 6.35 mm OD, ID of 4 mm, and a length of 2 cm. Catalyst powder was inserted into the tube held

in place by quartz wool packing on both the top and bottom of the vertical tube. Flow rates of the inlet gases were set by Porter mass flow meters and controlled by a Porter four-channel mass flow controller. Reactor temperature was controlled by an Omega CN6000 PID controller connected to a K-type thermocouple inserted directly adjacent to the catalytic bed within the heating zone.

Catalyst characterization

A Micromeritics Autochem 2920 catalyst characterization system was used to perform pulsed CO chemisorption to determine platinum dispersion. CO chemisorption was performed at 323 K and a CO/Pt ratio of 1 was assumed in the calculation of dispersion and subsequent particle size calculation. Transmission electron microscopy (TEM) and energy-dispersive x-ray (EDX) analysis were performed on an FEI Tencai F20 XT microscope using a Schottky field emitter electron source.

Steady state experiments

The catalyst was initially reduced in 5 % H_2/Argon mixture for 15 min at 673 K [8, 45, 46]. The catalyst was then conditioned in NO/O_2 environment (608 ppm/3.7 % vol.) with argon balance at 313 K at a space velocity of 59,000 h^{-1} [8]. The flow conditions for the experiments are based on typical LNT catalyst studies [47]. It should be noted that the pressure during passing through the catalyst was higher (1.701 bar) than atmospheric in order to overcome the dilution gas pressure.

To obtain steady state NO oxidation conversions, the reactor was ramped to temperature and held for 1 h at each steady state temperature. The conversion was measured in the range of temperatures from 473 to 773 K with 50 K temperatures increments. Pseudo-steady state profiles were obtained successively starting from the lowest temperature of 473 K. Following the 1 h steady state measurement, the reactor was then ramped at 10 K/min to the next temperature set point through the full temperature range.

Modeling

Global kinetic mechanism

Bhatia et al. proposed a global reaction model similar to this effort and proved that oxygen adsorption is the rate determining step using a micro-kinetic parametric study (validated by others groups [14–16, 18, 19, 28, 48]). Given the previously identified half order oxygen concentration dependence of NO oxidation, a new global reaction rate expression is derived here based upon the reaction mechanism in Eqs. 1–5.

The first step indicates that NO adsorption and desorption occurs with the forward and reverse rates equal to:

$$R_2 = k_2 p_{NO} \theta_{Pt} \tag{6}$$

$$R_{-2} = k_{-2} \theta_{Pt \cdot NO} \tag{7}$$

As oxygen adsorption is the rate determining step, these reactions are assumed to be in equilibrium, where the equilibrium constant equals:

$$K_{NO} = k_2 / k_{-2} \tag{8}$$

At the same time, dissociative oxygen adsorption and desorption on platinum occurs with the forward and reverse rates expressed as:

$$R_3 = k_3 p_{O_2}^{1/2} \theta_{Pt} \tag{9}$$

$$R_{-3} = k_{-3} \theta_{Pt \cdot O} \tag{10}$$

From the previous discussion, the authors assume that this step in the reaction is the rate determining step:

$$R_1 = R_{NO} = k_3 p_{O_2}^{1/2} \theta_{Pt} - k_{-3} \theta_{Pt \cdot O} \tag{11}$$

The third step of the reaction is the L–H oxidation reaction between adsorbed NO and atomic oxygen combined with the reverse reaction which is the dissociation of NO_2:

$$R_4 = k_4 \theta_{Pt \cdot NO} \theta_{Pt \cdot O} \tag{12}$$

$$R_{-4} = k_{-4} \theta_{Pt \cdot NO_2} \theta_{Pt} \tag{13}$$

with the equilibrium constant for the L–H step set as:

$$K_{LH} = k_4 / k_{-4} \tag{14}$$

In the next step, molecular nitrogen dioxide adsorption and desorption on platinum occurs with the forward and reverse rates expressed as:

$$R_5 = k_5 p_{NO_2} \theta_{Pt} \tag{15}$$

$$R_{-5} = k_{-5} \theta_{Pt \cdot NO_2} \tag{16}$$

The equilibrium constant expressed as:

$$K_{NO_2} = k_5 / k_{-5} \tag{17}$$

Solving Eqs. 6–8 and 12–17 results in:

$$\theta_{Pt \cdot O} = \frac{K_{NO_2} p_{NO_2} \theta_{Pt}}{K_{LH} p_{NO} K_{NO}} \tag{18}$$

The literature review illustrates that under most conditions, the surface is primarily covered with atomic oxygen and NO, leaving negligible vacant sites. As a

result, $1 = \theta_{Pt\cdot NO} + \theta_{Pt\cdot O}$ and NO_2 and O_2 surface coverage fractions are negligible. This outcome, combined with Eqs. 6, 7 and 18, results in the following expression for the available surface sites of Pt:

$$\theta_{Pt} = \frac{1}{\left(\frac{K_{NO_2} p_{NO_2}}{K_{LH} p_{NO} K_{NO}} + p_{NO} K_{NO}\right)} \tag{19}$$

Substituting Eqs. 18 and 19 into Eq. 11 yields:

$$R_{NO} = \left(k_3 p_{O_2}^{1/2} - k_{-3} \frac{K_{NO_2} p_{NO_2}}{K_{LH} p_{NO} K_{NO}}\right) \theta_{Pt} \tag{20}$$

Furthermore, incorporation of Eq. 19 into Eq. 20 results in:

$$R_{NO} = \frac{k_3 p_{O_2}^{1/2} (K_{LH} p_{NO} K_{NO}) - k_{-3} (K_{NO_2} p_{NO_2})}{\left[K_{NO_2} p_{NO_2} + (p_{NO} K_{NO})^2 K_{LH}\right]} \tag{21}$$

However, writing the global reaction rate as above does not account for the equilibrium limiting conditions at higher temperatures. Recalling the governing global reaction, Eq. 1, the forward and reverse reactions are:

$$R_1 = k_1 p_{NO} p_{O_2}^{1/2} \tag{22}$$

$$R_{-1} = k_{-1} p_{NO_2} \tag{23}$$

In equilibrium, the forward and backward rates are equal, which gives:

$$k_1 p_{NO} p_{O_2}^{1/2} = k_{-1} p_{NO_2}, \tag{24}$$

The equilibrium constant that can be calculated from Gibbs free energy equals:

$$K_{eq} = k_1 / k_{-1} \tag{25}$$

Substituting Eq. 24 into 25 gives:

$$K_{eq} p_{NO} p_{O_2}^{1/2} = p_{NO_2} \tag{26}$$

However, instead of substituting back the equilibrium constant from Eq. 26 directly into the NO oxidation reaction rate expression in Eq. 21, it can be modified using the properties of equilibrium for each detailed reaction step as proposed by Bhatia et al. [25]. The equilibrium constant for overall NO oxidation can be deduced as:

$$K_{eq} = K_{LH} \frac{K_{NO} K_{O_2}}{K_{NO_2}} \tag{27}$$

This can be modified as

$$\frac{K_{NO_2}}{K_{O_2}} = \frac{K_{LH}K_{NO}}{K_{eq}} \tag{28}$$

As a result, Eq. 21 can be written as:

$$R_{NO} = \frac{k_3 K_{NO} K_{LH}\left(p_{O_2}^{1/2} p_{NO} - \frac{p_{NO_2}}{K_{eq}}\right)}{\left[K_{NO_2} p_{NO_2} + \left(p_{NO} K_{NO}\right)^2 K_{LH}\right]} \tag{29}$$

Eq. 29 is the derived global reaction rate expression for NO oxidation with the combined molecular and dissociative adsorption of oxygen as the rate determining step.

Kinetic parameter values

The equilibrium constants used in Eq. 29 are derived from the kinetic theory of gases [7, 8, 31, 49, 50]. For NO adsorption–desorption, this is given as

$$K_{NO} = \frac{N_A A_{Pt} S_{NO}^0}{v_{NO}\left(2\pi W_{NO} R_u T_m\right)^{1/2}} \exp\left(-\frac{E_2 - E_{-2}}{R_u T_m}\right) \tag{30}$$

On the other hand, for NO_2 adsorption–desorption, it is given by:

$$K_{NO_2} = \frac{N_A A_{Pt} S_{NO_2}^0}{v_{NO_2}\left(2\pi W_{NO_2} R_u T_m\right)^{1/2}} \exp\left(-\frac{E_5 - E_{-5}}{R_u T_m}\right) \tag{31}$$

However, for the L–H reaction, the equilibrium constant is modified as:

$$K_{LH} = A_{LH} \exp\left[-\frac{(E_4 - E_{-4})}{R_u T_m}\right] \tag{32}$$

The pre-exponential factor for the L–H reaction step A_{LH} depends on the surface coverage of NO and atomic oxygen along with their proximity with respect to each other. Since the surface coverage and proximity depends on temperature, dispersion, etc., it cannot be directly determined from kinetic theory and is therefore calibrated.

The equilibrium constant for overall NO oxidation (K_{eq}) is derived from the Gibbs free energy at the catalyst temperature. The reaction rate coefficient for oxygen adsorption is modeled by the Arrhenius rate expression, where the pre-exponential factor is calculated from the kinetic theory of gases:

$$k_3 = A_3 \exp\left(-\frac{E_3}{R_u T_m}\right), \quad \text{with } A_3 = \frac{N_A S_{O_2}^0}{\left(2\pi W_{O_2} R_u T_m\right)^{1/2}} p^{1/2} \tag{33}$$

In the above equation, the value of A_3 is multiplied by the square root of the inlet pressure in order to ensure correct units for this parameter in the overall rate expression.

For Eqs. 30–33, values for the ideal gas constant, Avogadro's number, and molecular weight are commonly available in literature. The remaining parameters are evaluated based upon a literature review and their dependence on temperature and catalyst formulations (i.e., dispersion). Parameters that are taken to be independent of temperature and the catalytic surface are given in Table 1.

The sticking coefficient of NO is 0.9 which matches closely to 0.92 given by Olsson et al. [7, 8]. Bhatia et al. provided a sticking coefficient value at 0.85, Hauptman et al. indicated its value at 0.87 [14, 25], and Rankovic et al. used 0.88 [18, 19]. The sticking coefficient of NO_2 matches values given by Olsson et al. and Crocoll et al. and is close to the Rankovic et al. and Hauptman et al. value of 0.97 [7, 13, 14, 18, 19, 28].

The oxygen sticking coefficient depends upon temperature and surrounding species. Hence, the authors followed Campbell et al. and define the sticking coefficient as [31, 52]

$$S^0_{O_2} = S_{O_2} \exp\left(-\frac{E_{S,O_2}}{R_u T_m}\right) \tag{34}$$

Here S_{O_2} is 1.166×10^{-2} (−) and E_{S,O_2} is −4.029 (kJ mol^{-1}).

The desorption frequency (ν_{NO}) of NO matches the value given by Olsson et al., Crocoll et al., Hauptman et al., Bartram and Gorte [7, 8, 13, 14, 38, 39]. Also, the desorption frequency (ν_{NO_2}) of NO_2 is in line with Olsson et al. and Hauptmann et al.. However, it deviates from the 10^{13} value given by Crocoll et al. and Bartram et al. [7, 8, 13, 14, 39]. Adsorption activation energy for both NO and NO_2 is negligible as indicated by the literature [7, 8, 13–16, 18, 25].

The activation energy for the L–H reaction ranges from 101 to 124 kJ mol^{-1} in the literature apart from Crocoll et al. whom provide a low value of 35 kJ mol^{-1} [7, 13, 16–19, 25]. Hauptman et al. suggest the dependence of this activation energy on surface coverage of NO and Hgen. However, the authors have written the activation energy without surface coverage dependence in which is in agreement with the majority of previous studies [16, 17]. The chosen value of 101 kJ mol^{-1} is close to that of Olsson et al. and Rankovic et al. and not too dissimilar from Hauptman et al. if one neglects surface coverage effects [7, 16–19]. The activation energy of 51 kJ mol^{-1} for NO_2 decomposition (backward L–H reaction) is in line with 52.5 kJ mol^{-1} provided by Olsson et al. and 56 kJ mol^{-1} provided by

Table 1 Values of constant parameters

Parameters	Units	Values
A_{pt}	(m^2 site^{-1})	8×10^{-20} [51]
S^0_{NO}	(−)	0.9
ν_{NO}, ν_{NO_2}	(s^{-1})	1×10^{16}
E_2, E_5	(kJ mol^{-1})	0.00
$S^0_{NO_2}$	(−)	1
E_4	(kJ mol^{-1})	101
E_{-4}	(kJ mol^{-1})	51

Hauptman et al. after neglecting surface coverage effects [7, 8, 16, 17]. However, it is slightly higher than the Rankovic et al. value of 36.9 kJ mol^{-1} [18, 19]. The value chosen matches Crocoll et al. but they support the E-R mechanism [13].

Apart from the previously mentioned variables, there are three major parameters left to discuss: activation energy for desorption of NO and NO_2 and activation energy for oxygen adsorption. The literature illustrates that these three parameters depend on surface coverage and, in turn, on temperature and catalyst surface morphology. Hence, these parameters have been chosen to incorporate a functional dependency representative of the physical dependence on catalyst morphology; hereto known as Model 1.

NO adsorbs at room temperature [13], starts desorbing at 500 K, and near 550–600 K, desorbs completely [9, 25, 39]. At relatively high temperatures (>450 K), NO_2 dissociates promoting the formation of NO [13, 39]. This increases the surface coverage of NO, which reduces the activation energy of NO desorption [16]. Furthermore, the activation energy of NO desorption decreases with increasing oxygen surface coverage [13, 16]. It is commonly observed that NO_2 dissociation promotes a growth in oxygen surface coverage beyond oxygen self-promotion [8, 17, 24]. In the absence of NO_2 dissociation, oxygen tends to desorbs readily at high temperatures. In the case of oxygen surface coverage promotion by NO_2 dissociation, oxygen coverage increases relative to the higher temperature dissociation observed in the absence of reaction. This results in a reduction of the activation energy of NO desorption [53, 54]. The claim of a relative increase in surface coverage of oxygen with respect to temperature is independently supported by Wang and Yeh [41].

It is well known that the lack of surface species increases the activation energy of desorption of that respective species [8, 16, 17, 38, 39]. As discussed earlier, increasing the catalyst temperature decreases NO availability on the surface and some authors have even taken surface species coverage to be zero at high temperature. However, the literature review illustrates that oxygen surface coverage promotes NO desorption [13, 16, 17, 38, 39]. Hence, at high temperatures, the effect of desorption promotion by oxygen overtakes the decrease in desorption due to lack of species, subsequently promoting NO desorption (and lowering NO desorption activation energy).

When incorporating surface coverage effects, most authors write desorption activation energy as a function of surface coverage. However, this is not possible for a global reaction mechanism without modeling surface coverages independently. Therefore, temperature is used as a proxy for surface coverage based on the earlier discussion. The literature suggests that NO desorption activation energy is in the range of 90–140 kJ mol^{-1} [7–9, 11, 13, 14, 17, 25, 28]. Based on this information, the expression for NO desorption activation energy is formulated as:

$$E_{-2} = 115 - \alpha T_m \tag{35}$$

Here α is a constant used for calibration. Writing the activation energy in this manner will predict the highest activation energy for desorption at low temperatures that favors NO surface coverage and NO oxidation. Furthermore, at high

temperatures, decreased desorption activation energy will increase the probability of desorption without reaction, helping to satisfy the equilibrium condition. Finally, the calibrated parameter α directly serves as an indicator of the relative effect of the adapted parameter, where a larger α indicates increased importance of the surface coverage dependence term.

For the activation energy of NO_2 desorption, at low temperatures (<500 K), NO_2 decomposition is slower than NO oxidation and NO_2 desorption; thus, promoting NO_2 formation [7, 10, 13]. However, at higher temperatures (>550–600 K), the decomposition of NO_2 is preferred over desorption [13, 39]. In addition, around this temperature range, NO desorption is preferred over NO oxidation; thus, promoting decomposition of adsorbed NO_2 [39]. However, if the NO_2 decomposition is preferred and NO desorption is fast, than surface oxygen species should increase. This scenario is consistent with Hauptmann et al. finding an increase in PtO via the NO_2 dissociation reaction at temperatures >550 K [7, 8]. As the temperature increases, NO desorbs from the surface and reduces the possibility of NO_2 formation [39]. With a high decomposition rate and low surface concentrations of NO_2, it can be theorized that the decrease in observed surface NO_2 is a function of increased decomposition rate and an increase of NO_2 desorption activation energy is a function of the decrease in other surface species concentrations (change in surface concentrations of O_2 will be discussed later).

Therefore, this summary indicates that as the temperature increases, NO_2 struggles to form as a result of strong adsorption and decomposition, as well as changing surface coverage fraction of other components. This is represented by an increase NO_2 desorption activation energy modeled here as:

$$E_{-5} = 95 + \beta T_m \tag{36}$$

Here β is a constant used for calibration. In the literature, the activation energy of desorption is between 95 and 120 kJ mol^{-1}; hence, the authors have chosen the same range for the indicated expression [7, 8, 14, 16–19, 25].

Most important is the dependence of oxygen adsorption on catalyst morphology. Wang et al. show a direct correlation between heat of adsorption of oxygen and platinum particle size on alumina supported catalysts. It has also been shown that NO conversion is significantly increased with platinum particle size [41, 55]. This justifies the prior findings of higher NO conversions over larger platinum particles and the proposed correlation between oxygen adsorption and O_2 adsorption activation energy [7, 10, 13, 17, 18, 25]. Olsson et al., Bhatia et al., and Rankovic et al. all suggest the value of 30.4 kJ mol^{-1} that is used here with a slight modification [7, 18, 19, 25]. The particle size dependence of oxygen adsorption is included in the activation energy expression as such:

$$E_3 = 30.4 - \left(\frac{d_{Pt} - 5.9}{5.9}\right)\chi \tag{37}$$

Here the reference particle size of 5.9 nm is used based on Bhatia et al.'s findings [25].

Packed bed reactor model

Since the measurement of conversion took place at pseudo-steady state conditions, only the chemical species equation needs to be modeled for the packed bed reactor. Of note, the authors simulated a temperature ramp experiment after the kinetic model was calibrated and no difference was seen in the results.

Based on prior efforts of the third author [56], the chemical species equation for a packed bed simulation is equal to:

$$\varepsilon u_s \frac{\partial \bar{\mathbf{C}}}{\partial z} = \mathbf{D}^{eff} \frac{\partial^2 \bar{\mathbf{C}}}{\partial z^2} - G_{ca} \bar{\mathbf{R}} \tag{38}$$

Here the left hand side represents the advection of the molar species concentration $\left(\bar{\mathbf{C}}\right.$ as a function of the superficial velocity (εu_s). The indicated species concentrations include a combination of the two phases (surface and gas). The first term on the right hand side is the effective diffusivity that includes the porosity of the medium. The last term on the right hand side includes the influence of the reaction rates ($\bar{\mathbf{R}}$) on the surface along with a catalytic surface area per unit volume term (G_{ca}—$\mathrm{m}^2\ \mathrm{m}^{-3}$) in order to ensure the reaction rate expression (Eq. 29) is in the right units. This is used as an additional calibration variable since it cannot be readily measured.

Results and discussion

Fig. 1 shows the NO oxidation conversion profile with varying catalyst sintering temperatures. Conversion with sintering temperature varies substantially at temperatures below that which equilibrium conversion is reached. Above 604 K,

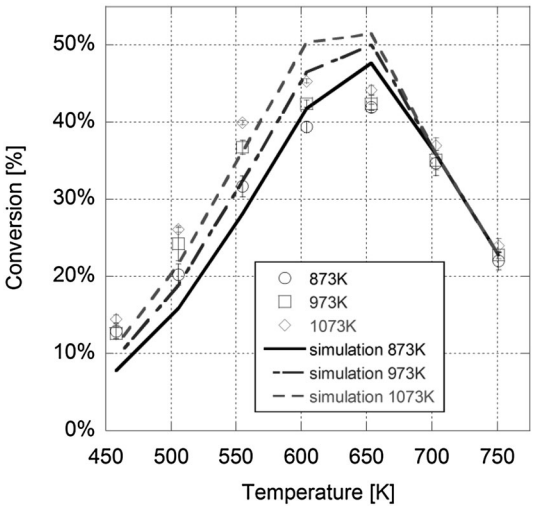

Fig. 1 Pseudo-steady state NO oxidation conversion versus temperature (both experimental and simulation) at isothermal conditions with varying catalyst sintering temperatures indicated (Model 1)

all catalysts demonstrate less than a 1.2 % variation in total conversion with the standard deviation averaging 0.9 %. These results illustrate that changing sintering conditions at these higher temperatures results in no significant change in conversion. This finding is further confirmed by prior literature findings; i.e., above 604 K, NO oxidation follows the equilibrium conversion curve and is independent of the catalyst aging conditions.

Fig. 1 also presents the results of the simulation efforts employing the adaptive kinetics model. Calibration of model parameters was accomplished using the Matlab *fmincon* routine while minimizing the least-squared curve-fit (LSQ) between the simulation results and the experimental data at each pseudo-steady state temperature.

The model is able to capture both the trends with temperature and dispersion at a relatively high accuracy with the model parameters given in Table 2. Furthermore, the equilibrium temperature limitation is accurately represented in the results.

Table 3 shows the platinum particle size for each of the sintered catalysts. As sintering temperature is increased from 873 to 1073 K platinum particle size is increases from 2.65 to 10.24 nm. As shown in Fig. 1, the increase in particle size results in higher NO oxidation conversions across all temperatures while the temperature of maximum conversion decreases with dispersion. For example, a maximum conversion of 45.3 % is achieved at 604 K over the catalyst sintered at 1073 K, whereas the catalyst with the smallest platinum particle size only achieved 41.9 % conversion at 654 K. This result is consistent with the literature for NO oxidation under oxidizing conditions, i.e. larger platinum particles have higher rates [10, 14, 25, 28, 35].

For NO oxidation below the equilibrium conversion temperatures, the change in conversion as a function of platinum particle size at each isothermal operating temperature is significant. Fig. 2 shows the impact of particle size on conversion at two individual isothermal operating temperatures (554 and 604 K) for both experimental data and those predicted by Model 1. The maximum variation in conversion with particle size is observed at 554 K, with an 8.2 % increase in conversion. Increasing the isotherm temperature to 604 K did not change the observed trend, but did result in a slight reduction of the percent increase in conversion to 5.9 %. While Model 1 accurately captures the trend of increasing

Table 2 Model 1 parameters specified or determined through calibration

Variable/parameter	Value
Packed bed particle dia. (μm)	0.0436
Bed pore diameter (μm)	0.0101
Packed bed void fraction (−)	0.4
Diffusivity model	Parallel pore
A_{LH} (−)	1.306×10^{-8}
G_{ca} (m^2 m^{-3})	1.306×10^{-11}
χ (−)	1.832
α	0.0292
β	0.0292

Table 3 Surface properties of the Pt/alumina catalyst

Sintering temperature (°C)	Dispersion (%)	Pt particle size (nm)
800	11.0	10.23
700	17.9	6.33
600	42.6	2.65

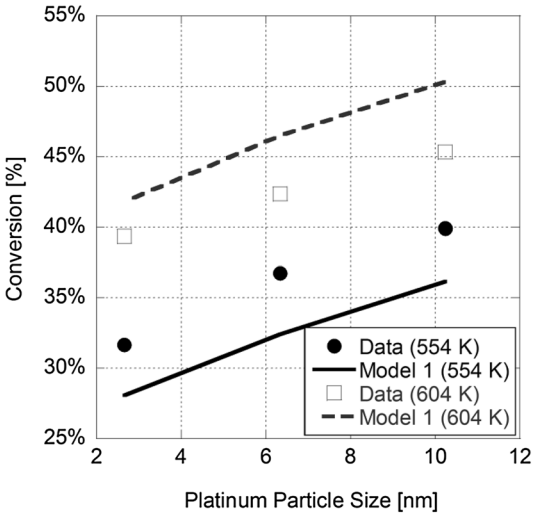

Fig. 2 Pseudo-steady state NO oxidation conversion versus particle size (both experimental and simulation) at isothermal conditions *black circle* 554 K *white square* 604 K

conversion with particle size, the absolute value of the conversion at each particle size deviates. This deviation is maintained through the range of reaction temperatures.

In comparison to previous literature modeling results, this simulation effort accurately portrays an increased maximum conversion while the temperature at which maximum conversion is achieved decreases as platinum particle size grows. These results support Bhatia et al.'s claim that surface coverage of NO has to be included in a global model for higher accuracy at lower temperatures [25]. Moreover, the results presented support the idea that oxygen adsorption is the rate determining step and that particles size effects must also be included in the expressions for desorption activation energy of NO and NO_2. A new expression was developed based upon the premise that adjacently adsorbed species affect the adsorption and desorption of NO and NO_2 substantially, where O_2 dominates the surface in the kinetically limited regime. Based upon this assumption, the authors used the changes in O_2 desorption profile with particle size as the basis for the model modification:

$$T_d = 476 + \frac{51}{d_{\mathrm{Pt}}} \tag{39}$$

and T_d modifies both the NO and NO_2 desorption activation energy expression as such when $T_m \geq T_d$:

$$E_{-2} = 115 - \alpha(T_m - T_d) \tag{40}$$

$$E_{-5} = 95 + \beta(T_m - T_d) \tag{41}$$

The expression in Eq. 39 has been developed based upon literature desorption profiles of oxygen, with surfaces coverages in the range of 0.5–0.7 ML over platinum single crystals where representative facets of platinum have been used to approximate well dispersed and non-dispersed platinum particles. In the case of well dispersed platinum, O_2-TPD from the Pt(100) surface shows an increased temperature of desorption, this is justified by the propensity of small platinum particles to undergo oxidation and subsequently have stronger Pt-O bonding [57]. To represent the non-dispersed platinum case, the authors reference O_2-TPD from the Pt(111) facet by Weaver et al.. On these surfaces, oxygen desorption occurs at the lowest temperature where desorption begins at 476 K [58]. The expressions defined in Eqs. 40 and 41 vary with temperature to approximate surface coverage effects, and are further modified by the platinum particle size effect incorporation defined by Eq. 39. It should be noted that no additional calibrated parameters are introduced with the adapted activation energy equations. In addition, the particle size dependence of the oxygen adsorption activation energy is retained from Eq. 37. The results from the modified version of Model 1 identified hence forth as Model 2 are presented in Fig. 3.

Fig. 3 shows the NO oxidation conversion profile with varying catalyst sintering temperatures compared with Model 2. In accordance with experimental data and Model 1, the conversion with sintering temperature does not vary at temperatures above the equilibrium limiting condition. Model 2 more accurately predicts catalyst aging effects on NO oxidation through the range of temperatures in the kinetically limited regime.

Model 2 shows substantial improvement over Model 1, evident in the LSQ value (Model 1 LSQ of 18.84, Model 2 LSQ of 6.43). The model accurately represents the

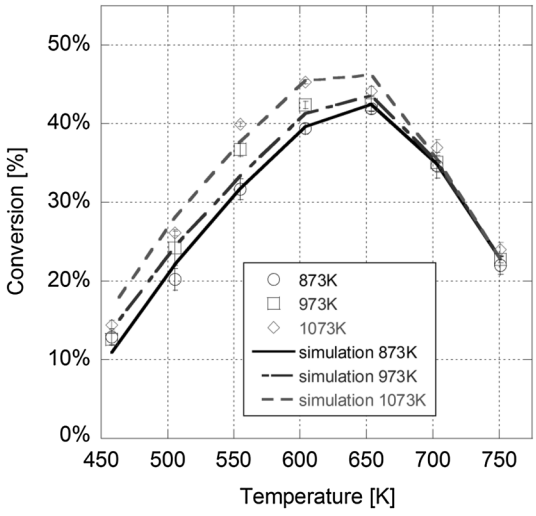

Fig. 3 Pseudo-steady state NO oxidation conversion versus temperature (both experimental and simulation) at isothermal conditions with varying catalyst sintering temperatures indicated (Model 2)

Table 4 Model 2 parameters specified or determined through calibration

Variable/parameter	Value
Packed bed particle dia. (μm)	0.0436
Bed pore diameter (μm)	0.0101
Packed bed void fraction (−)	0.4
Diffusivity model	Parallel pore
A_{LH} (−)	4.961×10^{-11}
G_{ca} (m^2 m^{-3})	6.753×10^{-12}
χ (−)	2.272
α	0.0237
β	0.0237

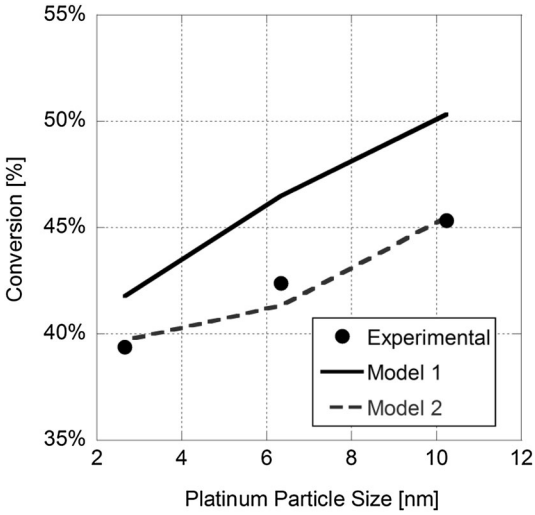

Fig. 4 Pseudo-steady state NO oxidation conversion versus particle size (both experimental and simulation) at 604 K

trend of decreasing maximum conversion temperature with increased platinum particle size. Table 4 shows the calibrated parameters for Model 2. It can be observed that χ increases from Model 1 to Model 2; whereas, both α and β decrease in Model 2 relative to Model 1.

It can be seen in Fig. 4 that Model 2 more accurately predicts the NO oxidation conversion at each of the platinum particle sizes. Model 2 also shows similar accuracy to Model 1 with respect to the relative change from the smallest to the largest particle size (slope of the line).

While detailed kinetics including surface coverage effects will more accurately simulate the conversion rate, the choice of modeling these effects through temperature dependencies provides a good compromise for a global kinetic approach. The kinetic parameters are within the range provided in the literature. Furthermore, the same kinetic parameters are used for multiple surface chemistries making the model truly global. This is important, because Stewart et al. have

demonstrated that there is significant change in prediction of conversion curves for different global models when compared to various surface morphologies [59].

Further improvements in the kinetic constants can be accomplished with additional experiments employing different inlet conditions (including water and other chemical species) and particle sizes. In addition, the global kinetics formulation presented can be utilized in a predictive manner prior to experimentation in order to help guide efforts.

Conclusions

Herein, an updated global kinetic model for NO oxidation is provided for a Pt/γ-alumina catalyst with direct applicability for OCs while helping provide insight into LNT operation. The majority of kinetic parameters are evaluated based on kinetic theory of gases. However, a select few are calibrated to fit experimental results for different catalyst morphologies. The values of the kinetic parameters all fall within previously reported in the literature values. The results illustrate the necessity of including NO surface coverage in the model (via a temperature analog) to simulate NO oxidation conversion at lower temperatures. The modification of the original modeling efforts clearly illustrate platinum particle size effects must be included to capture the effects of changing surface coverage with particle size.

The developed model accurately reflects that within the kinetic region, NO oxidation conversion increases with a decrease in dispersion (increase in platinum particle size) and, in the equilibrium region, NO oxidation conversion follows the equilibrium condition irrespective of the catalyst surface morphologies. Both of these results are consistent with the literature. Overall, the developed model predicts NO oxidation as a function of platinum particle size relatively well. Substantial improvement is achieved when the model is modified to include particle size effects on energies of desorption of NO and NO_2. The model is applicable for pre-reduced surfaces only for both OC and LNT devices. However, for an actual LNT device, NO oxidation occurs on the pre-reduced surface because of the previous regeneration event due to lean-rich cycling operation. Hence, the model provided is suitable for including in the simulation of an LNT after further efforts investigating the influence of NO_x storage materials on Pt particle size, dispersion, and NO oxidation are accomplished.

Acknowledgments This material is based upon work supported by the National Science Foundation under Award No. EPS-0903806 and matching support from the State of Kansas through Kansas Technology Enterprise Corporation. Financial support was also provided by the NSF IGERT C-CHANGE program at the University of Kansas.

References

1. Zelenka P (1996) Worldwide diesel emission standards, current experiences and future needs. Appl Catal B 10(1):3–28
2. Koltsakis G, Stamatelos A (1997) Catalytic automotive exhaust aftertreatment. Prog Energy Combust Sci 23(1):1–39

3. Chorkendorff I, Niemantsverdriet J (2007) Concepts of modern catalysis and kinetics, vol 1, 2nd edn. Wiley, New York
4. Johnson T (2008) Diesel engine emissions and their control. Platin Met Rev 52(1):23–37
5. Erkfeldt S, Jobson E, Larrson M (2001) The effect of carbon monoxide and hydrocarbons on NOx storage at low temperature. Top Catal 16/17(1–4):127–131
6. Epling WS et al (2004) Overview of the fundamental reactions and degradation mechanisms of NOx storage/reduction catalysts. Catal Rev 46(2):163–245
7. Olsson L et al (2001) A kinetic study of NO oxidation and NOx storage on Pt/alumina and Pt/BaO/alumina. J Phys Chem 105:6895–6906
8. Olsson L et al (1999) A kinetic study of oxygen adsorpion/desorption and NO oxidation over Pt/alumina catalysts. J Phys Chem 103:10433–10439
9. Bourane A et al (2001) Heats of adsorption of linear NO species on a Pt/alumina catalyst using in situ infrared spectroscopy under adsorption equilibrium. J Catal 204(1):77–88
10. Olsson L, Fridell E (2002) The influence of Pt oxide formation and Pt dispersion on the reactions of NO2 $\Leftrightarrow$ NO +1/2 oxygen over Pt/alumina and Pt/BaO/alumina. J Catal 210:340–353
11. Crocoll M, Weisweiler W (2004) Kinetische untersuchungen zur Pt-katalysierten oxidation von NO: modellierung und simulation. Chem Ing Tech 76(10):1490–1494
12. Epling W et al (2004) Overview of the fundamental reactions and degradation mechanism of NO_x storage/reduction catalysts. Catal Rev 46(2):163–245
13. Crocoll M, Kureti S, Weisweiler W (2005) Mean field modelling of NO oxidation over Pt/alumina catalyst under oxygen rich conditions. J Catal 229:480–489
14. Hauptmann W et al (2007) Global kinetic models for the oxidation of NO on platinum under lean conditions. Top Catal 42–43:157–160
15. Kromer B et al (2008) Modeling of NO oxidation and NO_x storage on Pt/BaO/alumina NO_x traps. Catal Today 136(1):93–103
16. Hauptmann W et al (2009) Inverse hysteresis during the NO oxidation on Pt under lean conditions. Appl Catal B 93(1):22–29
17. Hauptmann W et al (2009) A fast approach to predicitve models: NO-oxidation in exhaust gas aftertreatment systems. Top Catal 52:1925–1928
18. Rankovic N et al (2010) Extension of a kinetic model for NO oxidation and NO_X storage to fixed-bed Pt/Ba/alumina catalysts. Catal Commun 12(1):54–57
19. Rankovic N, Nicolle A, Da Costa P (2010) Detailed kinetic modeling study of NO_x oxidation and storage and their interactions over Pt/Ba/alumina monolith catalysts. J Phys Chem C 114:7102–7111
20. Sharma H, Mhadeshwar A (2012) A detailed microkinetic model for diesel engine emissions oxidation on platinum based diesel oxidation catalysts (DOC). Appl Catal B 127:190–204
21. Roy S, Baiker A (2009) NO_X storage-reduction catalysis: from mechanim and materials properties to storage-reduction performance. Chem Rev 109:4054–4091
22. Marques R et al (2004) Kinetics and mechanisms of steady-state catalytic NO + O_2 reactions on Pt/SiO_2 and Pt/$CeZrO_2$. J Mol Catal A 221:127–136
23. Mulla SS et al (2005) NO_2 inhibits the catalytic reaction of NO and oxygen over Pt. Catal Lett 100(3–4):267–270
24. Mulla S et al (2006) Reaction of NO and oxygen to nitrogen dioxide on Pt: kinetics and catalysts deactivation. J Catal 241:389–399
25. Bhatia D et al (2009) Experimental and kinetic study of NO oxidation on model Pt Catalysts. J Catal 266(1):106–119
26. Depcik C, Assanis D (2005) One-dimensional automotive catalyst modeling. Prog Energy Combust Sci 31:308–369
27. Wang TJ, Baek SW, Lee J-H (2008) Kinetic parameter estimation of a diesel oxidation catalyst under actual vehicle operating conditions. Ind Eng Chem Res 47(8):2528–2537
28. Olsson L, Blint R, Fridell E (2005) Global kinetic model for lean NO traps. Ind Eng Chem Res 44(9):3021–3032
29. Kim Y-D, Kim W-S (2009) Re-evaluation and modeling of a commercial diesel oxidation catalyst. Ind Eng Chem Res 48(14):6579–6590
30. Sampara CS, Bissett EJ, Chmielewski M (2008) Global kinetics for a commercial diesel oxidation catalyst with two exhaust hydrocarbons. Ind Eng Chem Res 47(2):311–322
31. Depcik C et al (2013) Adaptive global carbon monoxide kinetic mechanism over platinum/alumina catalysts. Catalyst 3(2):517–542

32. Konstantas GS, Stamatelos AM (2007) Modelling three-way catalytic converters: an effort to predict the effect of precious metal loading. Proc Inst Mech Eng 221:355–373
33. Cooper B, Thoss J (1989) Role of NO in diesel particulate emission control. Soc Automot Eng 890404:171–183
34. Gohndrone J, Masel RI (1989) A TPD study of nitric oxide decomposition on Pt(100), Pt(411) and Pt(211). Surf Sci 209(1–2):44–56
35. Xue E, Seshan K, Ross J (1996) Roles of support, Pt loading and Pt dispersion in the oxidation of NO–NO_2 and of SO–SO_2. Appl Catal B 11:65–79
36. Lee J-H, Kung H (1998) Effect of Pt dispersion on the reduction of NO by propene over alumina-supported Pt catalysts under lean-burn conditions. Catal Lett 51(1):1–4
37. Xue E, Seshan K, Ross JRH (1996) Roles of supports, Pt loading and Pt dispersion in the oxidation of NO–NO_2 and of SO_2–SO_3. Appl Catal B 11(1):65–79
38. Gorte RJ, Schmidt LD (1981) Binding states and decomposition of NO on single crystal planes of Pt. Surf Sci 109(2):367–380
39. Bartram M, Windham R, Koel B (1987) The molecular adsorption of nitrogen dioxide on platinum studied by TPD and vibrational spectroscopy. Surf Sci 184(1):57–74
40. Ovesson S et al (2005) NO oxidation properties of Pt(111) revealed by AB INITIO kinetic simulations. Phys Rev B 71:115406–115410
41. Wang C-B, Yeh C-T (1998) Effects of particle size on the progressive oxidation of nanometer platinum by dioxygen. J Catal 178(2):450–456
42. Gland J (1980) Molecular and atomic adsorption of oxygen on the Pt(111) and Pt(S)-12(111)x(111) surfaces. Surf Sci 93:487–514
43. Loof P et al (1993) Rapid sintering in NO of nanometre-sized Pt particles on alumina observed by CO temperature-programmed desorption and transmission electron microscopy. J Catal 144(1):60–76
44. Mahzoul H, Brihac JB, Gilot P (1999) Experimental and mechanistic study of NO_x adsorption over NO_x trap catalysts. Appl Catal B 20:47–55
45. Despress J et al (2004) Catalytic oxidation of nitrogen monoxide over Pt/silica. Appl Catal B 50:73–82
46. Dawody J et al (2005) Role of Pt-precursor on the performance of Pt/BaCO3/Al2O3.NO_x storage catalysts. J Mol Catal A 225:259–269
47. Clayton R et al (2009) Pt dispersion effects during NO_x storage and reduction on Pt/BaO/Al2O3 catalysts. Appl Catal B 90:662–676
48. Liu G, Gao P-X (2011) A review of NO_x storage/reduction catalysts: mechanism. Mater Degrad Stud Catal Sci Technol 1:552–568
49. Vannice A (2005) Kinetics of catalytic reactions. Springer, New York
50. White M (1990) Heterogeneous catalysis. Prentice Hall, Upper Saddle River
51. Anderson JR (1975) Structure of metallic catalysts. Academic Press, London
52. Campbell CT et al (1981) A molecular-beam investigation of the interactions of CO with a Pt(111) surface. Surf Sci 107:207–219
53. Elg AP, Eisert F, Rosen A (1997) The temperature dependence of the initial sticking probability of oxygen on Pt(111) probed with second harmonic generation. Surf Sci. 382(1):57–66
54. Tieber W, Athenstaedt W, Leisch M (1997) 3D-atom probe study of oxygen adsorpion on stepped platinum surfaces. Fresenius J Anal Chem 358:116–118
55. Benard S et al (2005) Supported platinum catalysts for NO oxidation sensors. Appl Catal B 55(1):11–21
56. Srinivasan A, Depcik C (2013) One-dimensional pseudo-homogeneous packed-bed reactor modeling: I. Chemical species equation and effective diffusivity. Chem Eng Technol 36(1):22–32
57. Shumber RB, Kan HH, Weaver JF (2007) Oxidation of Pt(111)-hex-R0. 7 by gas-phase oxygen atoms. Surf Sci 601(1):235–246
58. Weaver JF, Chen J-J, Gerrard AL (2005) Oxidation of Pt(111) by gas-phase oxygen atoms. Surf Sci 592(1–3):83–103
59. Stewart J et al (2012) Limitations of global kinetic parameters for automotive application. SAE Technical Paper 2012-01-1638